



HAL
open science

Structural variations in ϵ -type Al-Pd-(Mn, Fe) complex metallic alloy phases

Marc Heggen, Michael Engel, Sergiy Balanetsky, Hans-Rainer Trebin, M. Feuerbacher

► **To cite this version:**

Marc Heggen, Michael Engel, Sergiy Balanetsky, Hans-Rainer Trebin, M. Feuerbacher. Structural variations in ϵ -type Al-Pd-(Mn, Fe) complex metallic alloy phases. *Philosophical Magazine*, 2008, 88 (04), pp.507-521. 10.1080/14786430801894528 . hal-00513858

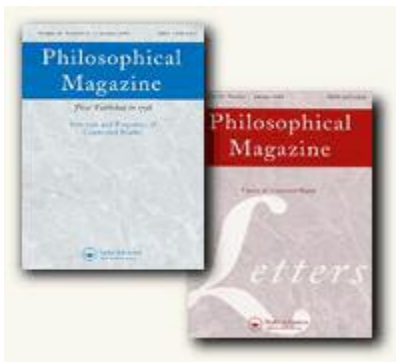
HAL Id: hal-00513858

<https://hal.science/hal-00513858>

Submitted on 1 Sep 2010

HAL is a multi-disciplinary open access archive for the deposit and dissemination of scientific research documents, whether they are published or not. The documents may come from teaching and research institutions in France or abroad, or from public or private research centers.

L'archive ouverte pluridisciplinaire **HAL**, est destinée au dépôt et à la diffusion de documents scientifiques de niveau recherche, publiés ou non, émanant des établissements d'enseignement et de recherche français ou étrangers, des laboratoires publics ou privés.



Structural variations in ϵ -type Al-Pd-(Mn, Fe) complex metallic alloy phases

| | |
|-------------------------------|---|
| Journal: | <i>Philosophical Magazine & Philosophical Magazine Letters</i> |
| Manuscript ID: | TPHM-07-Aug-0220.R1 |
| Journal Selection: | Philosophical Magazine |
| Date Submitted by the Author: | 29-Nov-2007 |
| Complete List of Authors: | Heggen, Marc; Forschungszentrum Juelich GmbH, Institut fuer Festkoerperforschung Engel, Michael; Universität Stuttgart, Institut für Theoretische und Angewandte Physik Balanetskyy, Sergiy; Forschungszentrum Juelich GmbH, Institut fuer Festkoerperforschung Trebin, Hans-Rainer; Universität Stuttgart, Institut für Theoretische und Angewandte Physik Feuerbacher, M.; Forschungszentrum Juelich GmbH, Institut fuer Festkoerperforschung |
| Keywords: | disclinations, phase transformations, plasticity of metals, TEM |
| Keywords (user supplied): | metadislocations, complex metallic alloys, tilings |
| | |



Structural variations in ϵ -type Al-Pd-(Mn, Fe) complex metallic alloy phases

Marc Heggen¹, Michael Engel², Sergiy Balanetsky¹,

Hans-Rainer Trebin², Michael Feuerbacher¹

1 Institut für Festkörperforschung, Forschungszentrum Jülich GmbH,

D-52425 Jülich, Germany

2 Institut für Theoretische und Angewandte Physik, Universität Stuttgart,

Pfaffenwaldring 57, D-70550 Stuttgart, Germany

Abstract

Structural modifications in complex metallic ϵ -Al-Pd-(Mn, Fe) samples are studied by means of transmission electron microscopy. The modifications were observed in the vicinity of metadislocations and at phase boundaries. They are determined by the density and inclination of phason planes. In the vicinity of metadislocations and at an ϵ_6 - ϵ_{28} -phase boundary, new monoclinic ϵ -type structures appear locally, which were not detected as bulk phases in Al-Pd-(Mn, Fe) before. The present work points out the close entanglement between defects, i.e. metadislocations and phason planes, and structural modifications in ϵ -type complex metallic alloys. An extended classification of ϵ -type phases including monoclinic phases is presented on the basis of two different tiling descriptions.

Keywords: Transmission Electron Microscopy; Tiling; Metadislocation; Complex Metallic Alloys

§ 1. Introduction

Several structurally related orthorhombic phases have been identified as ternary extensions of the Al_3Pd phase in the Al-Pd-(Mn, Fe) alloy systems [1-9]. They are observed in a composition range extending from the binary Al_3Pd phase to about 5 % Mn and 10 % Fe [9] and are termed ε -phases. They are denoted ε_l ($l = 6, 16, 22, 28, 34^1$) according to the index of the strong $(0\ 0\ l)$ diffraction spot which corresponds to the interplanar spacing of about 0.2 nm occurring in all of those phases [7-9]. ε -type phases are also found in the alloy systems Al-Pd-(Rh, Re, Ru, Co, Ir) and Al-Rh-(Ru, Cu, Ni) [9, 10].

In the literature, ε_l -phases are betimes referred to using alternative notations: The ε_6 - and ε_{28} -phases were denoted ξ' and Ψ , respectively [3-6]. Shramchenko and Denoyer [11] referred to the ε_6 -, ε_{16} -, and ε_{28} -phases as ξ' , ξ'_1 , and ξ'_3 . On the other hand, Engel [12] referred to these phases as ξ' , ξ'_1 , and ξ'_2 .

A particular feature of complex metallic ε -type phases is the occurrence of phase modulations and intermixing of structural elements. Modulated ε -type structures were observed in different alloy systems like Al_3Pd , $\text{Al}_{72}\text{Pd}_{25}\text{Cr}_3$, Al-Pd-Mn and Al-Pd-Fe [3, 10, 13].

In the present paper, structural modifications of ε -type phases in Al-Pd-(Mn, Fe) are studied by

1
2
3 means of transmission electron microscopy (TEM). We describe local structural modifications
4 related to the density and inclination of phason planes occurring at a phase boundary between ε_6 -
5 and ε_{28} -Al-Pd-Mn, where the phase boundary is built up by metadislocations. Furthermore
6 structural alterations in the vicinity of metadislocations in ε -type Al-Pd-Mn and Al-Pd-Fe
7 samples are studied. The presence of local unit cells corresponding to new monoclinic ε -type
8 phases is reported. These phase modulations are discussed in terms of two tiling models. A
9 generalized classification of ε -type structures is presented.
10
11
12
13
14
15
16
17
18
19
20
21
22
23

24 *Structural description*

25
26
27 The basic building blocks of all ε -phases are icosahedral-symmetric pseudo-Mackay clusters
28 which are arranged in columns along the [0 1 0] direction [4]. The projection of the column
29 centres on the (0 1 0) plane can be described in terms of so-called cluster tilings [1, 4, 14]. Two
30 different tiles are used, a flattened hexagon H and a combination of a nine-edged banana-shaped
31 polygon with a pentagon, termed phason line PL [3, 5]. Figure 1 a shows the H and PL tiles,
32 which are present in two different orientations, denoted H1, H2, PL1, and PL2. Figure 1 b and c
33 depict the tiling representations of the phases ε_6 and ε_{28} . These phases feature the orthorhombic
34 space group Pnma and C2mm, respectively [4, 24]. The ε_6 structure can be described by
35 alternating rows of H1 and H2 tiles [4]. The ε_{28} structure is characterised by additional PL1 tiles,
36 which are aligned in rows along the [1 0 0] direction (figure 1 c). An equivalent version of the ε_{28}
37 structure can be constructed using PL2 tiles. All ε_i phases have identical [1 0 0] and [0 1 0] lattice
38 constants, which, in the case of the Al-Pd-(Mn, Fe) alloy system, are $a = 2.35$ and $b = 1.66$ nm [4,
39 9]. The [0 0 1] lattice constants of the ε_i phases differ. The lattice constants of the phases ε_6 and
40
41
42
43
44
45
46
47
48
49
50
51
52
53
54
55
56
57
58
59
60

¹ The ε_{34} phase was only observed in the alloy system Al-Pd-Mn [9].

1
2
3
4 ε_{28} are related by a factor $3 + \tau$, where $\tau = \frac{1}{2}(\sqrt{5} + 1)$ is the irrational number of the golden mean
5
6 and $c(\varepsilon_6) = 1.23$ nm. Similar relations are found for other ε_l phases: The factor relating their [0 0
7
8 1] lattice constant to that of ε_6 are $1 + \tau$ (ε_{16}), $2 + \tau$ (ε_{22}), and $4 + \tau$ (ε_{34}).

9
10
11 In the present work all translation vectors are expressed in terms of the basis of ε_6 . Furthermore,
12
13 we will use the term ε -type phases not only for the phase sequence ε_l ($l = 6, 16, 22, 28, 34$), but
14
15 generalize it to all phases which can be described using the tiles H1, H2, PL1, and PL2 without
16
17 creating gaps or overlaps. This includes also the so-called ξ phase, which is structurally closely
18
19 related to ε_6 . It consists of a parallel arrangement of only one type of H tiles [4].
20
21
22
23

24
25 A mixture of structural elements belonging to different ε -type phases is observed in the vicinity
26
27 of metadislocations. These metadislocations are a new type of structural defect, which was first
28
29 observed in the ε_6 - and ε_{28} -phase [5, 15]. They are always associated to a certain number of
30
31 planar defects, so-called phason planes. A phason plane in the ε_6 -phase can be structurally
32
33 described by a row of PL-tiles along the [1 0 0] direction in an H-tile matrix. Since, on the other
34
35 hand, a row of PL tiles is a structural element of the ε_{28} -phase (cf. figure 1 c), the presence of
36
37 metadislocations leads to a mixture of structural features of the ε_6 - and the ε_{28} -phase [5, 16].
38
39
40
41

42
43 As an alternative to the cluster tiling involving H and PL tiles, other tilings can be used to
44
45 describe the structure of ε -type phases. The *rhomb tiling* [3, 12] offers a simpler geometrical
46
47 description than the cluster tiling. The relation between these alternative tilings is depicted in
48
49 figure 2 a. The cluster-tiles H and PL have an even number of vertices. Therefore, the vertices
50
51 can be divided into two disjoint sets (i.e. the cluster tiling is bipartite). By connecting the next-
52
53 neighbours of one of those sets the alternative tiling is obtained: H1/H2 are substituted by the
54
55 obtuse rhombs OR1/OR2, PL1 is substituted by a τ -inflated hexagon τ H, and PL2 is substituted
56
57
58
59
60

1
2
3 by a boat-shaped tile B (figure 2 a). This substitution is area-preserving, reversible and can be
4 applied to any cluster tiling representing an ε -type phase. The tiles B and τ H can be further
5
6 applied to any cluster tiling representing an ε -type phase. The tiles B and τ H can be further
7
8 decomposed into a combination of OR1, OR2, and an acute rhomb AR (figure 2 b). With this
9
10 decomposition step, the cluster tiling can be substituted by a tiling using only obtuse and acute
11
12 rhombs, OR1, OR2, and AR, and will then be referred to as a rhomb tiling [12]. The substitution
13
14 of the tile τ H by OR1, OR2, and AR, however, is not reversible as the back transformation is
15
16 ambiguous. For the classification of ε -type phases in this paper, representations in terms of the
17
18 cluster tiling and the rhomb tiling will be used.
19
20
21

22
23 In ε -type phases local rearrangements of cluster centres are possible. These can be represented in
24
25 the cluster tiling by an exchange and [0 0 1] displacement of PL1 and PL2 tiles (figure 2 c). This
26
27 local movement of PL tiles, involving a correlated rearrangement of atomic clusters, is called a
28
29 phason flip [3, 17]. Phason flips can also be described using the tiles OR1, OR2, B, and τ H
30
31 (figure 2 d) and the rhomb tiling (figure 2 e). In terms of the rhomb tiling, the distinction between
32
33 PL1 and PL2 tiles is not possible (figure 2 e). Accordingly, the substitution of the second and
34
35 third tiling of figure 2 c and d leads to equal rhomb tilings in figure 2 e.
36
37
38
39
40
41
42
43
44
45

46 § 2. Experimental details

47
48
49 An ε_6 -Al-Pd-Mn single crystal was grown by means of the Bridgman technique. The final
50
51 composition of the ingot was Al 73.6 at.%, Pd 22.1 at.%, Mn 4.3 at.%. It was characterised
52
53 metallurgically and oriented by Laue diffraction. The undeformed sample was investigated by
54
55 means of TEM and shows the presence of pure ε_6 -phase with a low density of defects like phason
56
57
58
59
60

1
2
3 planes. A sample of approximately $5 \times 2 \times 2 \text{ mm}^3$ in size was uniaxially deformed in compression
4
5 to about 0.5 % strain. According to previous investigations on the plastic deformation properties
6
7 of this material, the tests were performed in the ductile regime at a temperature of 700 °C. At
8
9 temperatures below about 650°C the material is brittle [23]. The long specimen axis,
10
11 corresponding to the compression direction, was oriented at an inclination of 45° with respect to
12
13 the [0 1 0] direction in order to provide favourable conditions (i.e. a high Schmid factor) for
14
15 metadislocation glide. The modes of metadislocation motion were discussed in detail by
16
17 Feuerbacher and Heggen [22]. After mechanical testing the sample was quenched on a cold metal
18
19 plate and prepared for TEM by standard techniques. The microstructural investigation was
20
21 performed using a JEOL 4000 FX microscope and a Philips CM 200 FEG microscope equipped
22
23 with a spherical-aberration corrector [18]. ϵ_6 - as well as ϵ_{28} -phase regions, formed during plastic
24
25 deformation, were observed. The phase boundary region between both phases was analysed.
26
27 Furthermore, structural modifications around metadislocations were analysed. A centric aperture
28
29 around the direct beam and the central spots was used for imaging, which leads to enhanced
30
31 contrast between phason-line elements and hexagon-type structural elements.
32
33
34
35
36
37

38
39 The second sample studied, an Al-Pd-Fe cast of the initial composition Al 64.4 at.%, Pd 34.8
40
41 at.%, Fe 1.5 at.%, was heat treated at 750 °C for 980 h. The material was characterised by
42
43 scanning electron microscopy and TEM. The sample contains crystalline parts of ϵ -type phase
44
45 with a composition Al 72.0 at.%, Pd 22.8 at.%, Fe 5.2 at.%. Lattice-fringe images under bright-
46
47 field Laue conditions were taken in a JEOL 4000 FX microscope using a centric aperture around
48
49 the direct beam and the central spots. The TEM samples were oriented along the [0 1 0] direction.
50
51 In the present investigation two differently processed materials were compared: Plastically
52
53 deformed single crystalline Al-Mn-Pd and cast polycrystalline Al-Mn-Fe. It is shown, however,
54
55
56
57
58
59
60

1
2
3 that the structural properties of metadislocations are not dependent on selective processing of the
4
5 samples.
6
7
8
9
10

§ 3. Microstructural investigations

11
12
13
14 Figure 3 shows an electron micrograph of a phase boundary between the ϵ_6 - (left-hand side) and
15 the ϵ_{28} -phase (right-hand side) in the Al-Pd-Mn sample. The ϵ_{28} -phase shows a darker contrast
16 and the regular stacking of phason planes, visible as dark lines, can be seen in the rightmost part
17 of the micrograph (cf. figure 1 c). The course of selected groups of phason-plane segments is
18 indicated by curved lines. The phase boundary is formed by an almost straight-line arrangement
19 of metadislocations along the [0 0 1] direction. Exemplarily, the core of one metadislocation with
20 16 phason planes is indicated by an arrow. Another metadislocation, distant from the phase
21 boundary by about 200 nm is indicated by an arrowhead. In the ϵ_{28} -phase, at a distance from the
22 phase boundary the phason planes are oriented closely along the [1 0 0] direction, while closer to
23 the boundary they are mostly curved and inclined with respect to the [1 0 0] direction.
24
25
26
27
28
29
30
31
32
33
34
35
36
37
38

39 Electron-diffraction patterns were taken in the vicinity of the phase boundary from three different
40 regions, indicated by circles in figure 3. The sample regions a and c are located in the ϵ_6 - and ϵ_{28} -
41 phase, respectively, and b corresponds to a region in the direct vicinity of the phase boundary on
42 the ϵ_{28} -side, about 50 nm distant from the metadislocations. The corresponding diffraction
43 patterns are shown in figure 4. The insets show enlargements corresponding to the area marked
44 by a rectangle in figure 4 a. For a closer inspection of the diffraction patterns, figures 4 b and c
45 show additionally further enlarged segments. The diffraction patterns 4 a and c confirm the
46 presence of the ϵ_6 - and ϵ_{28} -phase. The corresponding (0 0 6) and (0 0 28) reflections are marked.
47
48
49
50
51
52
53
54
55
56
57
58
59
60
60

1
2
3 of the reflection positions, four diffraction spots are marked by circles in figure 4 c. These
4 positions are transferred to the inset in figure 4 b (circles). The low-intensity diffraction spots in
5 the inset of figure 4 b show slight deviations with respect to position and intensity from those of
6 the ϵ_{28} -phase.
7
8
9
10

11
12
13 Figures 5 a and b show high-resolution micrographs of the Al-Pd-Mn sample in two regions close
14 to the ϵ_6 - ϵ_{28} -phase-boundary corresponding to area b in figure 3. The micrographs were taken at
15 an overfocus of about 40 nm in order to emphasise the large spatial frequencies, which gives rise
16 to bright-contrast dots at the centres of the pseudo-Mackay clusters. A tiling representation of
17 these areas using H1, H2, PL1, and PL2 tiles can then easily be made by connecting the bright
18 dots. The tilings which consist of semi-transparent white H1 and H2 and red PL1 and PL2 tiles
19 are superimposed to the micrographs. In the tiling representation of figure 5 a, the unit-cell
20 projection of the ϵ_{28} -phase is represented by a rectangle. Over large areas of the micrograph,
21 however, the ϵ_{28} -structure is disordered. Phason planes are not strictly oriented along the [1 0 0]
22 direction but show a wavy course due to mixing of PL1 and PL2 tiles within a single phason
23 plane (e.g. regions 1 and 2 in figure 5 a). This observation can be explained by the occurrence of
24 phason flips within a phason plane (cf. figure 2 c). In some areas the phason planes are inclined,
25 i.e. a (1 0 1) translation can be found between neighbouring equal PL tiles (arrows). Along the [0
26 0 1] direction a varying number of H1 and H2 tiles is observed between two PL tiles, ranging
27 from 0 to 3 in figure 5 a (examples are indicated by circles).
28
29
30
31
32
33
34
35
36
37
38
39
40
41
42
43
44
45
46
47
48
49

50 In figure 5 b an average separation of phason planes larger than in the ideal ϵ_{28} -phase is observed.
51 Locally, a rectangular cell is spanned by the vectors (1 0 0) and (0 0 $4+\tau$) representing the ϵ_{34} -
52 phase (rectangle in figure 5 b). At the top right part of figure 5 b two neighbouring PL tiles of a
53 phason plane are related by a (1 0 2) translation (arrow). In some areas even stronger inclinations
54
55
56
57
58
59
60

1
2
3 between PL tiles are observed.
4

5
6 A lattice fringe image of the same sample showing structural modifications around
7
8 metadislocations is presented in figure 6. Four metadislocations (labelled 1 to 4) are connected to
9
10 ϵ_6 -phase regions (labelled 5 to 8) [5]. Phason lines are visible as dark features. The course of
11
12 selected groups of phason-plane segments is indicated by curved lines. They show a variable
13
14 inclination with respect to the [1 0 0] direction. For example, in an area close to the ϵ_6 -phase
15
16 region (labelled 9) phason planes join, which have a negative and positive slope with respect to
17
18 the [1 0 0] direction. Furthermore, a variable density of phason planes is observed in terms of
19
20 their mutual distance along the [0 0 1] direction. The variation of the phason plane density is
21
22 introduced due to the presence of metadislocations. These metadislocations terminate phason
23
24 planes and therefore lead to an unidirectional compaction of the latter. As an example, phason
25
26 planes terminating at a the metadislocation labelled 3 are indicated by curved lines in figure 6.
27
28 The phason plane density on the left hand side of the metadislocation is much higher than at the
29
30 right hand side. In addition to the phason planes, a stacking fault (10) is observed on the right
31
32 hand side of figure 6. This type of defect was discussed by Klein *et al.* [15], but is not a matter of
33
34 discussion in the present investigation.
35
36
37
38
39
40
41

42 The local structure of some selected areas in this sample region is analysed in figure 7 a to c,
43
44 which depict enlargements of the boxed regions of figure 6. Within areas of 10 to 20 nm in
45
46 diameter, homogeneous local structures are observed, which can be matched by tilings. In figure
47
48 7 a, a space-filling tiling is made using PL and H tiles. The corresponding unit cell is spanned by
49
50 the vectors (1 0 0) and (0 0 3+ τ). This local structure can therefore be identified as ϵ_{28} phase. The
51
52 local structure in figures 7 b and c is characterised by inclined phason planes and different
53
54 numbers of H1 and H2 tiles between the phason planes. The unit cell is spanned by the vectors (1
55
56
57
58
59
60

0 -1) and (0 0 4+ τ) (figure 7 b), and (1 0 1) and (0 0 6+ τ) (figure 7 c), respectively. The angle between those vectors is 108° and 72° rather than 90°. The lattice can therefore be considered a monoclinic rather than an orthorhombic lattice.

A similar structural study was made using an Al-Pd-Fe sample. Figure 8 shows a lattice fringe image in the vicinity of metadislocations (labelled 1 and 2), which are connected to ξ -phase regions (labelled 3 and 4) [19]. The course of selected groups of phason-plane segments is indicated by curved lines. Again, they show a variable inclination with respect to the [1 0 0] direction, and a variable density of phason planes is observed. Figures 9 a to c depict enlargements of the boxed regions in figure 8, which are matched by cluster tilings. In figure 9 a the corresponding unit cell is spanned by the vectors (1 0 0) and (0 0 1+ τ). This local structure can be identified as ϵ_{16} phase. In figures 7 b and c the unit cell is spanned by the vectors (1 0 -1), (0 0 4+ τ) and (1 0 -1), (0 0 2+ τ), respectively.

§ 4. Discussion

Microstructural investigations

In this paper, a TEM study on structural modifications in complex metallic ϵ -type phases is presented. These structural modifications are connected to phason defects and metadislocations and occur on different length scales. For instance, figures 5 a and b show structural modifications, i.e. phason flips, on the scale of the lattice parameter. Single PL elements exhibit a modulated behaviour within the phason planes which are, on average, oriented along the [1 0 0] direction. Beyond that, figure 3, 6, and 8 demonstrate that structural modulations exist on a larger

1
2
3 scale ranging from some tens to hundreds of nanometres. They depend on the curvature and
4
5 density of phason planes in these areas.
6
7

8
9 On the unit-cell scale, local structural disordering was observed at an ϵ_6 - ϵ_{28} -phase boundary by
10
11 means of high-resolution TEM. Various distances between phason planes along the [0 0 1]
12
13 direction and the local occurrence of other unit cells (e.g. ϵ_{34}) were found. The average structure
14
15 in the vicinity of the phase boundary has a larger separation between the phason planes than the
16
17 perfect ϵ_{28} -phase. Single PL elements are moved out of regularly stacked (0 0 1) planes by
18
19 phason flips which results in a wavy course of the phason planes (figure 5). In addition, the
20
21 electron diffraction investigation reveals structural modulations in the direct vicinity of the phase-
22
23 boundary region. The shifts of spots can be related to the presence of phason disorder [20, 21].
24
25
26

27
28 On a larger scale structural modifications are connected to the course of phason planes which are
29
30 observed as dark lines in figure 3. Metadislocations terminating the phason planes are not ideally
31
32 stacked along [0 0 1] direction, but may be distant from the boundary along the [1 0 0] direction
33
34 (see arrowhead in figure 3). Accordingly, the density of phason planes varies locally and, on
35
36 average, increases gradually from the ϵ_6 - to the ϵ_{28} -phase region. As ϵ -type phases within a
37
38 sequence ϵ_l ($l = 6, 16, 22, 28, 34$) are distinguished by their [0 0 1] lattice constants, i.e. the
39
40 distance between phason planes along the [0 0 1] direction, the variation of the phason plane
41
42 distance due to the presence of metadislocations is associated with local structural variations. No
43
44 sharp phase boundary but rather a transient region is observed between related ϵ -type phases. The
45
46 intermediate region is characterized by a variation of the phason plane density leading to a
47
48 continuous phase change and the presence of phason disorder.
49
50
51
52
53
54

55
56 Structural modulations connected to the course of phason planes were furthermore investigated in
57
58 the vicinity of metadislocations in an Al-Pd-Mn and an Al-Pd-Fe sample (figures 6 to 9). Due to
59
60

1
2
3 the presence of metadislocations, phason planes are geometrically forced to circumvent defected
4 areas (for example the ones labelled 8 in figure 6). This gives rise to various phason-plane
5 inclinations with respect to the [1 0 0] direction. Furthermore, the introduction of additional
6 phason planes by metadislocations (for example the ones labelled 3 in figure 6) causes a local
7 variation of the phason plane density and to a local structural variation within the sequence of ε_l -
8 phases ($l = 6, 16, 22, 28, 34$). The structural variations around the metadislocations are found in
9 both samples investigated here, the plastically deformed single crystalline Al-Mn-Pd and cast
10 polycrystalline Al-Mn-Fe sample. These observations are not dependent on selective processing
11 of the samples.

12
13 The observation of phason plane inclinations with respect to the [1 0 0] direction leads a
14 structural description in terms of a tiling model which is elaborated in the following subsection.
15 These local phason plane inclinations can be described in terms of monoclinic ε -type structures.
16 The discussion in terms of monoclinic structures is based on the structural investigation within
17 the (0 1 0)-plane. Potential structural changes along the [0 1 0]-direction are not considered.
18 Monoclinic ε -type bulk phases have not been observed in the Al-Pd-(Mn, Fe) alloy system
19 before.

20
21 An important characteristic regarding structural modifications connected to metadislocations in ε -
22 type phases is the mutual sense of the terms “defect” and “structural element”. Phason planes
23 associated with metadislocations are defects, but, on the other hand, they are elements of the ideal
24 structure in all ε -type phases but ε_6 . In this sense, the presence of defects is always necessarily
25 connected to structural variations of the surrounding material and to the local appearance of new
26 monoclinic structures around the defects.

Classification of ε -type phases

In figure 10, a systematic classification scheme for ε -type orthorhombic and monoclinic phases is presented. PL1 and PL2 tiles are depicted white, H1 and H2 tiles dark grey and light grey, respectively. The presented ε -type structures are characterized by different periodic arrangements of straight phason planes. They differ with respect to their inclination along the $[1\ 0\ 0]$ direction and their spacing along the $[0\ 0\ 1]$ direction.

The central column of the figure represents the tilings of the orthorhombic ε -phases. From top to bottom we find ε_{16} , ε_{22} , ε_{28} , ε_{34} , and ε_{40} . Their lattice vectors, expressed in terms of the basis of ε_6 (cf. §1; the basis vectors are shown in figure 2b), are given by $(1\ 0\ 0)$ and $(0\ 0\ z+\tau)$, $z = 1, 2, 3, 4, 5, \dots$. The first, second, fourth, and fifth column of figure 10 show ε -type tilings of monoclinic structures spanned by $(1\ 0\ -2)$, $(1\ 0\ -1)$, $(1\ 0\ 1)$, and $(1\ 0\ 2)$ translation vectors, respectively. Note that the structures in corresponding columns on the left and right hand side are related by a mirror operation. Tilings shown in the same row possess the same translation vector along the $[0\ 0\ 1]$ direction; tilings in the same column possess the same inclination of phason planes.

The tilings shown in figure 10 can be classified by two indices (m, n) according to the translation vectors $(0\ 0\ m+1+\tau)$ and $(1\ 0\ n)$, with $m = 0, 1, 2, 3, \dots$ and $|n| \leq m$. The index n is confined corresponding to the latter relation in order to avoid overlap of the tiles. For reasons of presentation, the phases $(3, -3)$, $(4, -3)$, $(4, -4)$, etc. were not shown in figure 10. Orthorhombic and monoclinic phases are classified by the indices $n = 0$ and $n \neq 0$, respectively. The ε_6 -phase and the ξ -phase, consisting only of H tiles, can be expressed in terms of the present classification as the limit of an infinite distance between the phason planes, i.e. by the indices $(n, 0)$ and $(n, \pm n)$ for $n \rightarrow \infty$, respectively.

1
2
3 In terms of this classification, the orthorhombic structures shown in figure 7 a and 9 a correspond
4 to the orthorhombic phases referred to as (2,0) and (0,0). The monoclinic structures depicted in
5 figure 7 and 9 can be assigned to the structures (3,-1) (figure 7 b and fig. 9 b), (4,1) (figure 7 c),
6 and (1,-1) (figure 9 c). It should be noted that the enlarged areas in figure 7 and 9 were selected
7 to show locally undistorted ε -type structures which can be classified according to the scheme of
8 figure 10. In these areas, the local structures remain constantly ordered over distances of several
9 lattice parameters. The intermediate ranges between such areas show mixing of structural
10 elements of related ε -phases. The same holds for areas showing heavily curved phason planes
11 around metadislocations or rapidly changing phason-plane density at phase boundaries. These
12 local changes take place by a high density of phason flips.

13
14
15
16
17
18
19
20
21
22
23
24
25
26
27
28 Hiraga [13] studied decagonal and quasicrystalline phases by high-resolution electron
29 microscopy in Al-Pd-(Cr, Co, Fe). He observed modulated ε -type structures, which can be
30 classified according to our scheme. The areas shown in figure 11 of Hiraga's work can be
31 identified as (3,1), (2,-1), (2,0), and (0,0) [13].

32
33
34
35
36
37
38 A comparable classification can be created in terms of the rhomb tiling. The unit cell is spanned
39 by the basis vectors \mathbf{a} and \mathbf{c} , while \mathbf{b} is the (fixed) basis vector perpendicular to the tiling plane.
40 The vectors \mathbf{a} and \mathbf{c} are given by integer linear combinations of the three vectors \mathbf{e}_i , $i = 1, 2, 3$,
41 that span the rhomb tiles OR, AR (cf. figure 2). In contrast, the edges of the cluster tiling are
42 described by a regular five-star basis. In this sense the rhomb tiling is a geometrically simpler
43 description than the cluster tiling. The vector \mathbf{c} connects two PL tiles in the [0 0 1] direction,
44 while the vector \mathbf{a} connects two next-neighbouring PL tiles along or inclined with respect of the
45 [1 0 0] direction. In the $\{\mathbf{e}_i\}$ basis they are
46
47
48
49
50
51
52
53
54
55
56
57
58
59
60

$$\mathbf{c} = \begin{pmatrix} 1 \\ 2+m \\ 1 \end{pmatrix} \text{ and } \mathbf{a} = \begin{pmatrix} 1 \\ n \\ -1 \end{pmatrix} . \quad (1)$$

The classification in terms of the rhomb tiling is shown in figure 11. OR1 and OR2 tiles are depicted white and AR tiles grey. The parameter m specifies the distance of the phason planes, and the parameter n the inclination of the phason planes with respect to the $[0\ 0\ 1]$ direction. The lattice constants a , c , and their angle ϕ can be calculated as a function of m , n :

$$c/\lambda = \tau + 1 + m, \quad (2)$$

$$a/\lambda = \sqrt{n^2 + 2 + \tau}, \quad (3)$$

$$\tan \phi = \frac{\sqrt{2 + \tau}}{n}, \quad (4)$$

for $n \neq 0$ and $\lambda = c(\varepsilon_6) = 1.23$ nm. For $n = 0$ $\phi = 90^\circ$ holds.

The number of the H1, H2, and PL tiles per unit cell is $\#(\text{H1}) = m + n$, $\#(\text{H2}) = m - n$, $\#(\text{PL}) = 2$.

The parameters m , n can be determined by counting the relative densities of the tile types:

$$m = \frac{\#(\text{H1}) + \#(\text{H2})}{\#(\text{PL})}, \quad n = \frac{\#(\text{H1}) - \#(\text{H2})}{\#(\text{PL})}. \quad (5)$$

A direct consequence of these relations is the restriction $|n| \leq m$.

It should be noted that the phases of the present classification scheme represent “simple” phases which can be built with the tiles H1, H2, PL1, and PL2 in the sense that they are described by two translation vectors connecting PL tiles. This results in structures which are characterised by a uniform distribution of straight phason lines. However, more complex periodic phases using H and PL tiles can be constructed, e.g. by the creation of supercells of the presented simple phases.

Acknowledgments

We thank Dipl.-Ing. C. Thomas and M. Schmidt for the materials production. This work was supported by the Deutsche Forschungsgemeinschaft (PAK 36), and the 6th Framework EU Network of Excellence "Complex Metallic Alloys" (Contract No. NMP3-CT-2005-500140).

For Peer Review Only

References

- [1] M. Audier, M. Durand-Charre, and M. de Boissieu, *Phil. Mag. B* **68**, 607 (1993).
- [2] Y. Matsuo, K. Hiraga, *Phil. Mag. Lett.* **70**, 155 (1994).
- [3] H. Klein, M. Audier, M. Boudard, M. de Boissieu, L. Beraha, and M. Duneau, *Phil. Mag.* **73**, 309 (1996).
- [4] M. Boudard, H. Klein, M. de Boissieu, M. Audier, and H. Vincent, *Phil. Mag. A* **74**, 939 (1996).
- [5] H. Klein, M. Feuerbacher, P. Schall, and K. Urban, *Phys. Rev. Lett.* **82**, 3468 (1999).
- [6] H. Klein, M. Durand-Charre, and M. Audier, *J. All. Comp.* **296**, 128 (2000).
- [7] M. Yurechko, A. Fattah, T.Y. Velikanova, and B. Grushko, *J. Alloys & Comp.* **329**, 173 (2001).
- [8] S. Balanetsky, B. Grushko, T.Y. Velikanova, and K. Urban, *J. All. Comp.* **376**, 158 (2004).
- [9] M. Yurechko, B. Grushko, T.Y. Velikanova, and K. Urban, "Phase Diagrams in Materials Science", Proceedings of the 6th International School-Conference, PDMS VI-2001, Ed. T.Y. Velikanova, 92-97 (2004).
- [10] S. Balanetsky, B. Grushko, and T.Y. Velikanova, *Z. Kristallogr.* **219**, 548 (2004).
- [11] N. Shramchenko, and F. Denoyer, *Eur. Phys. J. B* **29**, 51-59 (2002).
- [12] M. Engel, H.-R. Trebin, *Phil. Mag.* **85**, 2227 (2005).
- [13] K. Hiraga, "The structures of decagonal and quasicrystalline phases with 1.2 nm and 1.6 nm periods, studied by high-resolution electron microscopy", Proceedings of the International Conference on Aperiodic Crystals, Aperiodic 94, Eds. G. Chapius and W. Paciorek, Les

1
2
3 Diablerets, Switzerland, 341-350 (1994).

4
5
6 [14] M. Engel, H.-R. Trebin, *Phil. Mag.* **86**, 979 (2006).

7
8
9 [15] H. Klein and M. Feuerbacher. *Phil. Mag.* **83**, 4103 (2003).

10
11
12 [16] M. Heggen and M. Feuerbacher, *Phil. Mag.* **86**, 985 (2006).

13
14
15 [17] L. Beraha, M. Duneau, H. Klein, and M. Audier, *Phil. Mag. A* **76**, 587 (1997).

16
17
18 [18] M. Haider, H. Rose, S. Uhlemann, B. Kabius, and K. Urban, *Nature* **392**, 768 (1998).

19
20
21 [19] M. Feuerbacher, M. Heggen, and S. Balanetsky, in preparation.

22
23
24 [20] P.M. Horn, W. Malzfeldt, D.P. DiVincenzo, J. Toner, and R. Gambino, *Phys. Rev. Lett.* **57**,
25
26 1444 (1986).

27
28
29 [21] V. Franz, M. Feuerbacher, M. Wollgarten, and K. Urban, *Phil. Mag. Lett.* **79**, 333 (1999).

30
31
32 [22] M. Feuerbacher, and M. Heggen, *Phil. Mag.* **86**, 985 (2006).

33
34
35 [23] M. Feuerbacher, H. Klein, and K. Urban, *Phil. Mag. Lett.* **81**, 639 (2001).

36
37
38 [24] F. J. Edler, thesis, Diss. ETH Nr. 12384, ETH Zuerich (1997).

Figure captions

Figure 1: Hexagon H1/H2 and phason-line tiles PL1/PL2 (a) are the basic building blocks of ε -type phases; examples are the ε_6 -phase (b) and the ε_{28} -phase (c).

Figure 2: (a) The cluster tiles (light grey) can be substituted by the tiles OR1/OR2, τ H, and B. (b) The tiles τ H and B (grey) can be further decomposed into obtuse rhombs OR1/OR2 and acute rhombs AR. Local rearrangements of tiles (phason flips) can be formed in the cluster tiling (c), the tiling using the tiles OR1/OR2, τ H, and B (d), and the rhomb tiling (e).

Figure 3: Transmission electron micrograph of a phase boundary in Al-Pd-Mn formed by metadislocations between the ε_6 -phase on the left and the ε_{28} -phase on the right hand side. Phason planes associated to the metadislocations can be observed as dark lines. One metadislocation is marked by an arrow. Diffraction patterns were taken at the sample areas a, b, and c.

Figure 4: Diffraction patterns of the sample areas a, b, and c of figure 3. The insets show enlarged images of the boxed section.

Figure 5: High resolution micrographs of an Al-Pd-Mn sample in the ε_{28} -phase region close to the ε_6 - ε_{28} -phase-boundary. The corresponding cluster tilings are superimposed to the micrographs.

Figure 6: Lattice fringe image of an Al-Pd-Mn sample containing four metadislocations (1 to 4) connected to ξ -phase regions (5 to 8). The course of phason planes is exemplarily indicated by curved line elements (9, see text). In addition a stacking fault is observed (10). Enlarged images of the boxed regions are presented in figure 7.

1
2
3
4
5
6
7
8
9
10
11
12
13
14
15
16
17
18
19
20
21
22
23
24
25
26
27
28
29
30
31
32
33
34
35
36
37
38
39
40
41
42
43
44
45
46
47
48
49
50
51
52
53
54
55
56
57
58
59
60

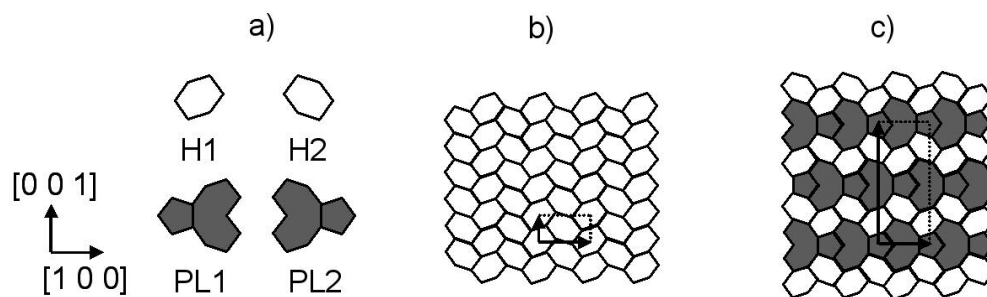
Figure 7: Enlarged sections of the areas marked a, b, and c in figure 6. The local structure is matched by three different cluster tilings.

Figure 8: Lattice-fringe image of an Al-Pd-Fe sample containing two metadislocations (1 and 2) connected to ξ -phase regions (3 and 4). The course of phason planes is exemplarily indicated by curved line elements. Enlarged images of the boxed regions are presented in figure 9.

Figure 9: Enlarged sections of the areas marked a, b, and c in figure 8. The local structure is matched by three different cluster tilings.

Figure 10: Classification of ε -type phases using the cluster tiling. The phases are characterized by two indices (m, n) with $m = 1, 2, 3, \dots$ and $|n| \leq m$. See text.

Figure 11: Classification of ε -type phases using the rhomb tiling. The tilings of figure 10 and 11 are related by a substitution.

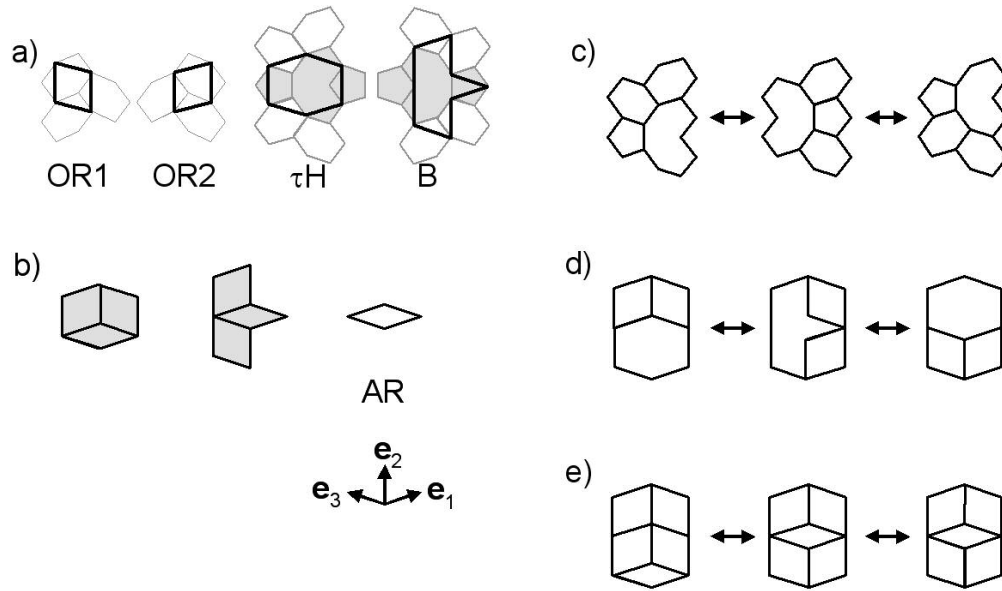


18 **Hexagon H1/H2 and phason-line tiles PL1/PL2 (a) are the basic building blocks of ϵ -type**
 19 **phases; examples are the ϵ_6 -phase (b) and the ϵ_{28} -phase (c).**

20 419x131mm (72 x 72 DPI)

21
22
23
24
25
26
27
28
29
30
31
32
33
34
35
36
37
38
39
40
41
42
43
44
45
46
47
48
49
50
51
52
53
54
55
56
57
58
59
60

Peer Review Only



(a) The cluster tiles (light grey) can be substituted by the tiles OR1/OR2, τH, and B. (b) The tiles τH and B (grey) can be further decomposed into obtuse rhombs OR1/OR2 and acute rhombs AR. Local rearrangements of tiles (phason flips) can be formed in the cluster tiling (c), the tiling using the tiles OR1/OR2, τH, and B (d), and the rhomb tiling (e).

411x242mm (72 x 72 DPI)

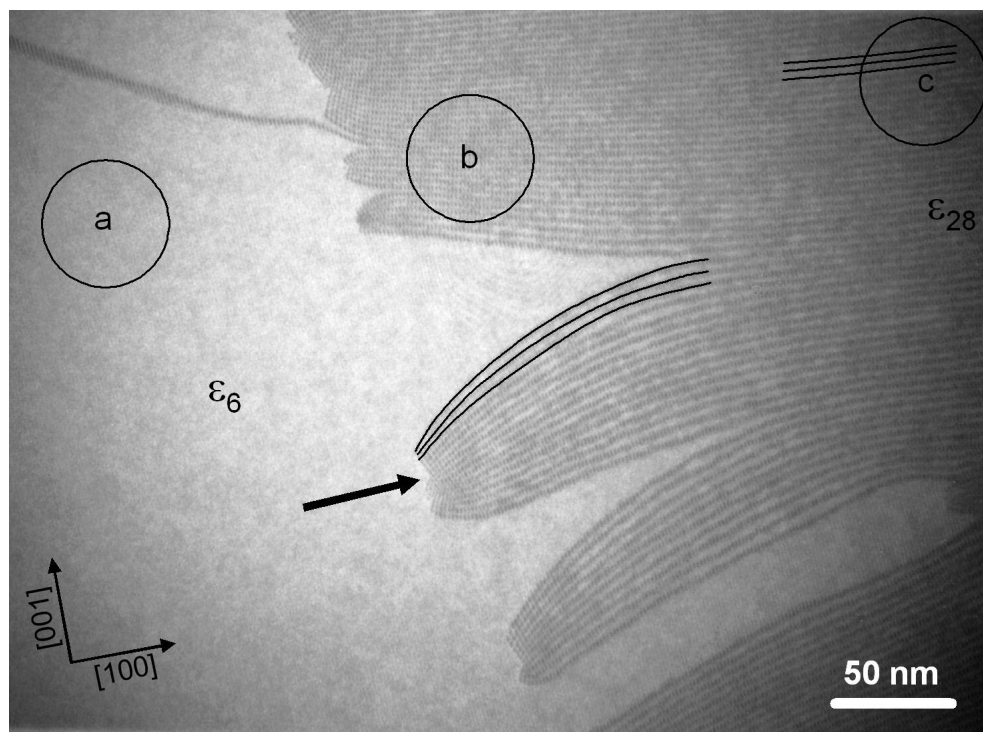
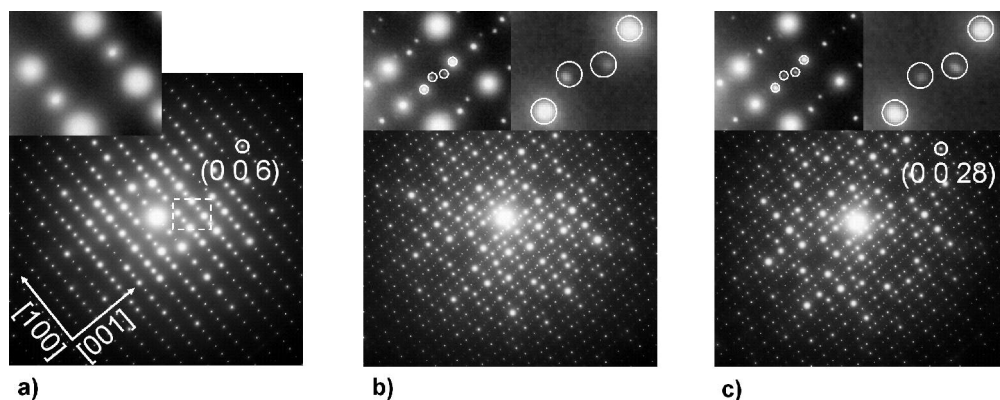


Figure 3: Transmission electron micrograph of a phase boundary in Al-Pd-Mn formed by metadislocations between the ϵ_6 -phase on the left and the ϵ_{28} -phase on the right hand side. Phason planes associated to the metadislocations can be observed as dark lines. One metadislocation is marked by an arrow. Diffraction patterns were taken at the sample areas a, b, and c.
529x385mm (72 x 72 DPI)



Diffraction patterns of the sample areas a, b, and c of figure 3. The insets show enlarged images of the boxed section.

925x367mm (72 x 72 DPI)

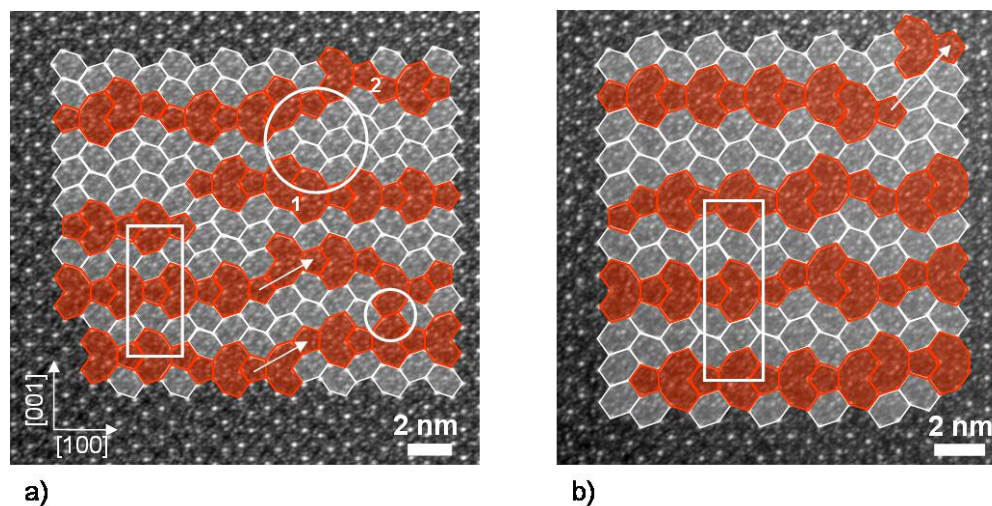
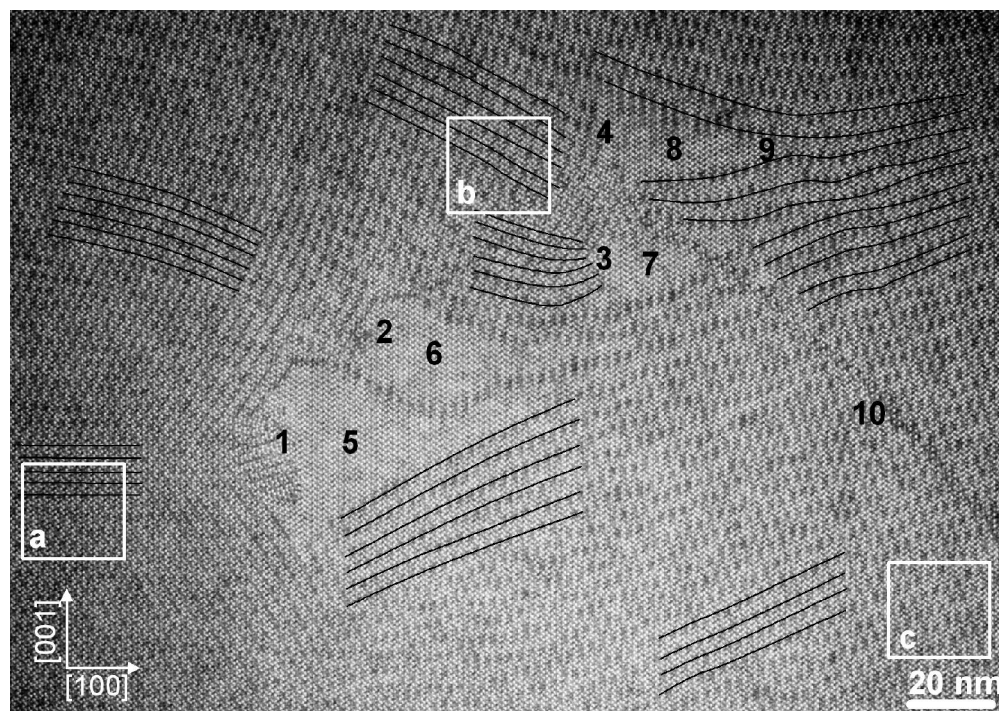


Figure 5: High resolution micrographs of an Al-Pd-Mn sample in the ϵ_{28} -phase region close to the ϵ_6 - ϵ_{28} -phase-boundary. The corresponding cluster tilings are superimposed to the micrographs.



Lattice fringe image of an Al-Pd-Mn sample containing four metadislocations (1 to 4) connected to ξ -phase regions (5 to 8). The course of phason planes is exemplarily indicated by curved line elements (9, see text). In addition a stacking fault is observed (10). Enlarged images of the boxed regions are presented in figure 7.

667x472mm (72 x 72 DPI)

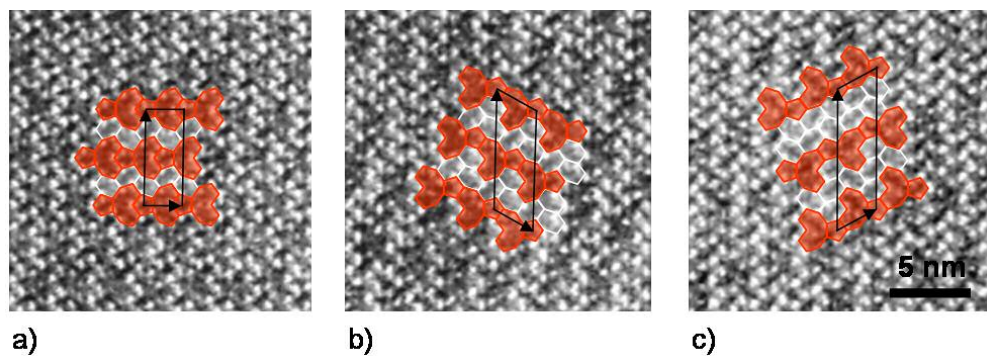
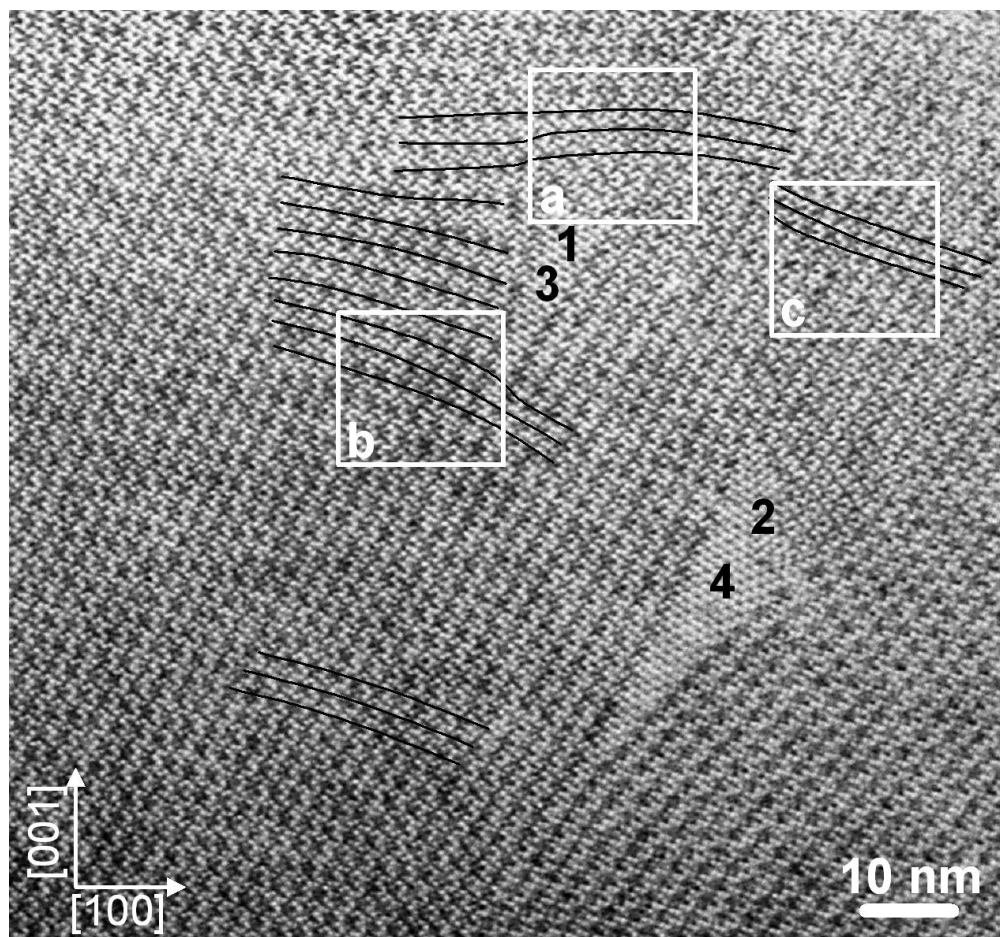


Figure 7: Enlarged sections of the areas marked a, b, and c in figure 6. The local structure is matched by three different cluster tilings.



Lattice-fringe image of an Al-Pd-Fe sample containing two metadislocations (1 and 2) connected to ξ -phase regions (3 and 4). The course of phason planes is exemplarily indicated by curved line elements. Enlarged images of the boxed regions are presented in figure 9.

447x417mm (72 x 72 DPI)

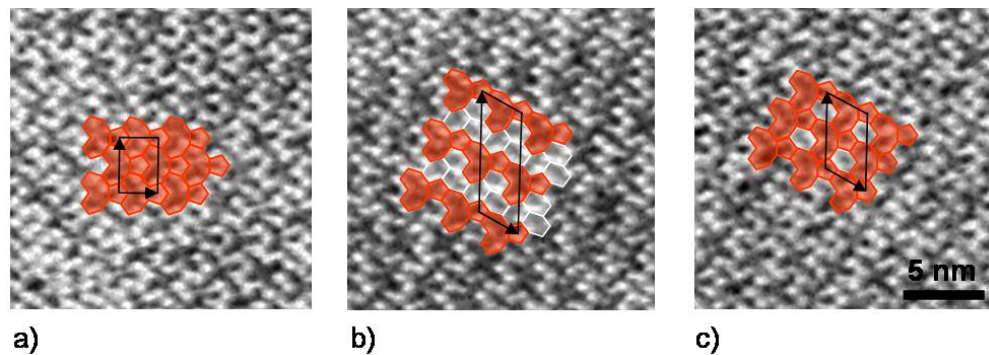
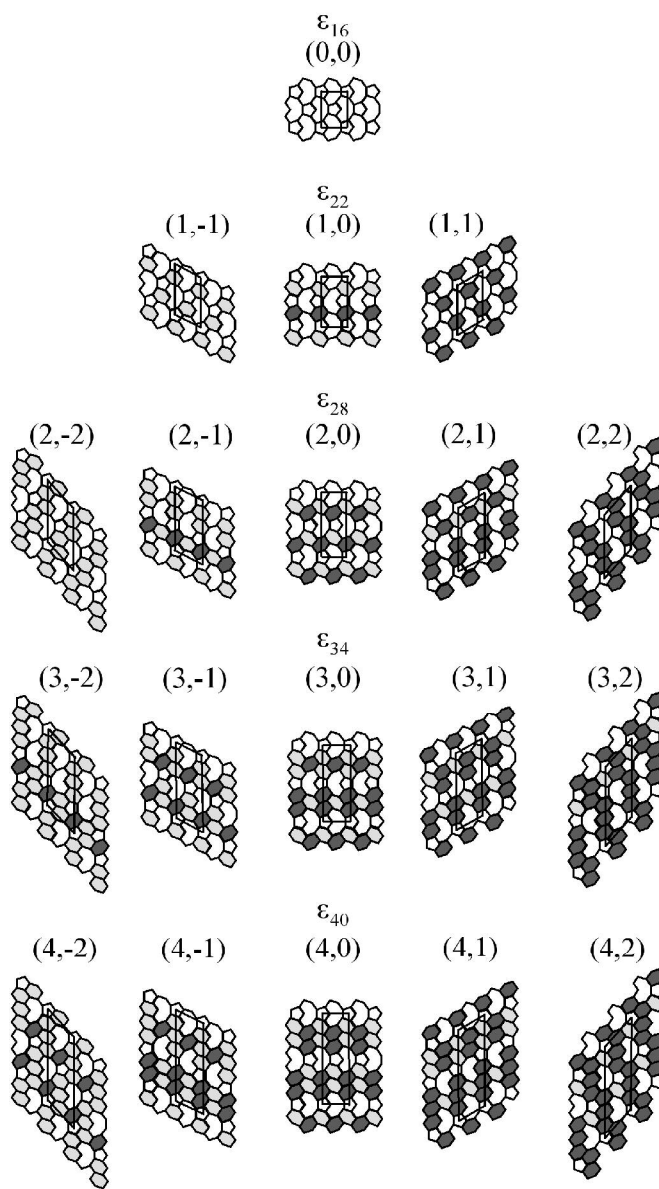


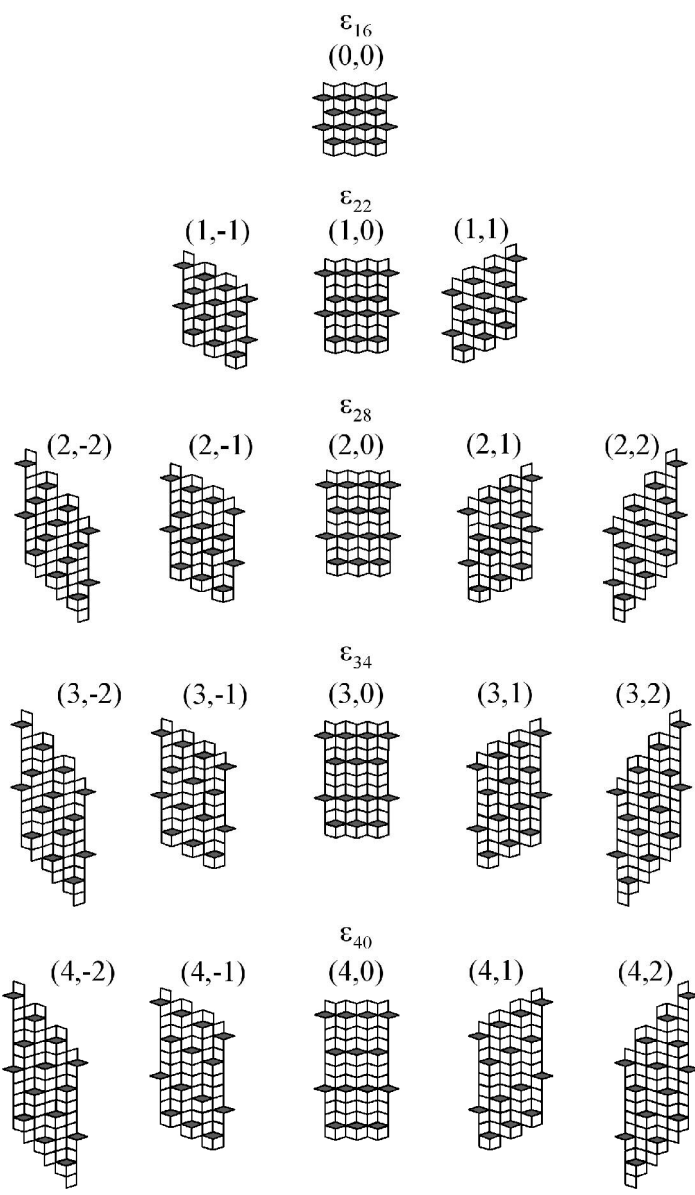
Figure 9: Enlarged sections of the areas marked a, b, and c in figure 8. The local structure is matched by three different cluster tilings.



Classification of ϵ -type phases using the cluster tiling. The phases are characterized by two indices with $m = 1, 2, 3, \dots$ and $|n| \leq m$. See text.

582x1062mm (72 x 72 DPI)

1
2
3
4
5
6
7
8
9
10
11
12
13
14
15
16
17
18
19
20
21
22
23
24
25
26
27
28
29
30
31
32
33
34
35
36
37
38
39
40
41
42
43
44
45
46
47
48
49
50
51
52
53
54
55
56
57
58
59
60



Classification of ϵ -type phases using the rhomb tiling. The tilings of figure 10 and 11 are related by a substitution.
623x1061mm (72 x 72 DPI)